 doi:10.20944/preprints201907.0206.v1

Article

Structural, Magnetic and Mössbauer Studies of Ga and Zr Doped $Dy_2Fe_{17-x}Zr_x$ and $Dy_2Fe_{16}Ga_{1-x}Zr_x$ (x=0.00, 0.25, 0.50, 0.75, 1.00)

Jiba Nath Dahal [1,*] and K. S. Syed Ali [2]

[1] Department of Physics, University of California Merced, Merced, CA 95343
[2] Department of Science, Harmony Science Academy, 12005 Forestgate Dr. Dallas, TX-75243
* Correspondence: jdahal@ucmerced.edu

Abstract: The substitution of Zr and Ga in Dy_2Fe_{17} was found to have an important effect on their structure and magnetic properties. The Rietveld analysis confirmed that the crystalline system wereTh_2Ni_{17} structure. Lattice parameters *a* (Å) and *c* (Å), unit cell volume (Å^3), bonding distance (Å) were calculated by using Rietveld analysis. The unit cell volume of $Dy_2Fe_{17-x}Zr_x$ and $Dy_2Fe_{16}Ga_{1-x}Zr_x$ increase linearly with the Zr and Ga substitution. The substitution of Zr and Ga are limited up to x=1 to avoid the decrease in saturation magnetization. The Curie temperature (Tc) of $Dy_2Fe_{17-x}Zr_x$ and $Dy_2Fe_{16}Ga_{1-x}Zr_x$ are found to be Zr content dependent. The maximum curie temperature was observed 510K. x = 0.75 for $Dy_2Fe_{17-x}Zr_x$ and 505.1 K, x = 0.5 for $Dy_2Fe_{17-x}Zr_x$ which are 102 K and 97 K higher than Dy_2Fe_{17}. The room temperature Mössbauer analysis shows the decrease average hyperfine field and increases the isomer shift with Zr doping.

Keywords: permanent magnetic materials; 2:17 intermetallic; X-ray diffraction; rietveld analysis; Mössbauer Spectroscopy; curie temperature; soft magnet; doping

1. Introduction

Intermetallic compounds (rare-earth elements (R) and 3d-transition elements (T)) possess outstanding magnetic properties because of their high saturation magnetization (Ms). R_2Fe_{17} compounds were studied in late the 1970s and the values of $(BH)_{max}$ and Coercivity (Hc) were found about 26 MGOe and 15 kOe respectively but they have very low Curie temperature (~473 K for Gd_2Fe_{17} and ~300 K for Dy_2Fe_{17}) and low magnetic anisotropies [1]. Many researches have been done to improve the curie temperatures of Dy_2Fe_{17} [2–4] either by replacing the Fe atoms with non-magnetic atoms (Al, Si, Ga) [5] or by doping refractory atoms (Ti, V, Mo, Nb, W, Zr) in Fe site [6–10]. It is also found that substitution of magnetic atoms such as (Co, Ni, Cr, Mn, Ni) [11], non-metals such as C, N, and H in R_2Fe_{17} lattice also increase the curie temperature of R_2Fe_{17} compounds. [12–15]. The substitution of non-magnetic atoms at Fe sites has been reported to increase ferromagnetic coupling which in turn increases the Curie temperature [16-17]) and magneto-crystalline anisotropy [18]. The introduction of nitrogen on interstitial sites of $R_2Fe_{17}N_x$ also increased the Curie temperature. This happened because of volume expansion and increase of the distance of iron atoms which changes the magnetic properties of R_2Fe_{17} compounds [19,20]. Betancourt *et al* (2003) [21] reported that Zr and Nb substitution can also improve magnetic properties. The curie temperatures of Ce_2Fe_{17} [22], Gd_2Fe_{17} [5] Dy_2Fe_{17} [8], Pr_2Fe_{17} [23], etc., are improved by the addition of elements like Si, Cr, Mn, and Ga. The substitution of the non-magnetic atom into the R_2Fe_{17} brings the concomitant decrease in magnetization which affects the energy product of the permanent magnets [18]. Furthermore, it is possible to increase the magnetic moment *via* Fe-Zr 3d band hybridization which can bring band narrowing or increase exchange splitting by moving the 3d↑ states below the Fermi level or allow charge transfer out of the 3d band, provided the spin-down density of states exceed the spin-up density [24]

Preprints (www.preprints.org) | NOT PEER-REVIEWED | Posted: 17 July 2019 doi:10.20944/preprints201907.0206.v1

The present work focusses on replacing the Fe atom by elements, Zr and Ga into the Dy_2Fe_{17}. The substitution of the non-magnetic atom was limited to up to x= 1 to prevent a significant reduction in saturation magnetization. Doping of Zr and Ga atoms can increase the lattice parameter *a*, *c* and unit cell volume and can also improve Fe-Fe exchange interaction.

2. Experimental

The raw materials of Dy, Fe, Zr and Ga were used with ~99.9% of purity and purchased from Sigma Aldrich. The samples $Dy_2Fe_{17-x}Zr_x$ and $Dy_2Fe_{16}Ga_{1-x}Zr_x$ (x = 0.00, 0.25, 0.50, 0.75, 1.00) were prepared via arc melting technique in a high purity argon atmosphere. The ingots were melted several times to ensure homogeneity. The prepared alloys were made into fine powders and the X-ray powder data sets were collected using Bruker (D8 Advance) diffractometer with the monochromatic incident beam of CuK_α (λ~1.5406 Å) radiation with the 2θ range from 20° to 70° with the step size of 0.042°. The XRD analysis was performed by the well-known refinement Rietveld method [25] using the JANA2006 [26] software package. The purpose of this refinement process is to minimize the difference between the theoretically modeled profile and the observed ones as a function, $\sum_{hkl} W_{hkl} \ (|F_o| - |F_c|)^2$ where W_{hkl} is the weight assigned to each observation and F_O and F_C are the observed and calculated structure factors.

Magnetic properties of the powder sample were investigated at room temperature (RT) using vibrating sample magnetometer (VSM) in the maximum field of 1.2T. To minimize the effect of the demagnetizing field, the samples were compacted at 3000psi and cut into rectangular parallelepiped with the ratio of length to a width larger than three times and embedded in epoxy. A modified thermogravimetric analyzer (DuPont 910) equipped with a permanent magnet was used to determine the Curie temperature of composite samples.

The Mössbauer spectra of the samples were obtained at RT using a 25 mCi ^{57}Co source in Rh foil mounted on a constant acceleration drive system (SEE Co. Minneapolis, USA) in transmission geometry. The velocity scale of the Mössbauer spectrometer was calibrated by measuring the hyperfine field of α-Fe foil, at room temperature. The Mössbauer spectra were analyzed using the WMoss software from SEE Co. The spectra were least-square fitted with the hyperfine field (HF), isomer shift (IS) and quadrupole shift (QS) as variables.

3. Results and Discussions

Figure 1(a) and **(b)** represent the raw XRD powder profile of $Dy_2Fe_{17-x}Zr_x$ and $Dy_2Fe_{16}Ga_{1-x}Zr_x$ (x = 0.00, 0.25, 0.50, 0.75, 1.00). **Figure 2** represents the representative Rietveld refinement profile for $Dy_2Fe_{16}Ga_{0.75}Zr_{0.25}$. The Rietveld [25] fittings reveal a nice matching of the observed and calculated profiles for both systems. A small additional phase $DyFe_3$ was observed for x=1 Zr content. During the refinement process, the scale, structural parameters, lattice parameters, peak shift, preferred orientation, background profile functions, thermal parameters, surface roughness were refined until the observed XRD profile matches well with the calculated profile. The initial crystal structure parameters were used as given by Liao et al. [27]. In the hexagonal setting, Dy was fixed at the 2*b* (0, 0, 0.25) and 2*d* (0.333, 0.667, 0.75) site and Fe was fixed at 4*f*(0.333 0.667 0.105), 6*g*(0.5 0 0), 12*j*(0.333 0.969 0.25), and 12*k*(0.167 0.333 0.985). The profile was constructed using a pseudo-Voigt function. Profile asymmetry was introduced by employing the multi-term Simpson rule integration devised by Howard [28]. A surface roughness correction was also applied using the Pitschke, Hermann, and Matter [29] model. **Table 1** shows the refined structural parameters for both for $Dy_2Fe_{16-x}Zr_x$ and $Dy_2Fe_{16}Ga_{1-x}Zr_x$. From **Table 1**, the refined results confirmed that the unit cell volume ($Å^3$) increases with x-content. The plot for lattice parameters *a, c* and unit cell volume (V) are shown in **Figure 3 (a)** and **3(b).** This increase in volume maybe because of bigger atom Ga (r_{ionic} = 136 pm) and Zr (r_{ionic} =206 pm) sitting at the smaller iron (r_{ionic} = 126pm) atom site. The increasing lattice parameters confirmed that both Zr and Ga addition to the host lattice has been done properly. **Table 2** represents, the site occupancy table for $Dy_2Fe_{17-x}Zr_x$ and $Dy_2Fe_{16}Ga_{1-x}Zr_x$, which shows the Zr atom occupies all 4f, 6g, 12j

Preprints (www.preprints.org) | NOT PEER-REVIEWED | Posted: 17 July 2019 doi:10.20944/preprints201907.0206.v1

and 12k sites but the 12j and 12k sites are mostly impacted with the Zr substitution (**Figure 4(a)**), the site occupancy of Zr and Ga for $Dy_2Fe_{16}Ga_{1-x}Zr_x$ are plotted in **Figure 4(b)** and the values are presented in **Table 2**. From these results, both Zr and Ga atoms prefer to be in 12j and 12k sites with a minimum affinity for 4f and 6g sites [30,31] and the increase in Zr occupancy and the decrease in Ga occupancy at 12j and 12k site shows that Zr atom is replaced by Ga atom in $Dy_2Fe_{16}Ga_{1-x}Zr_x$.

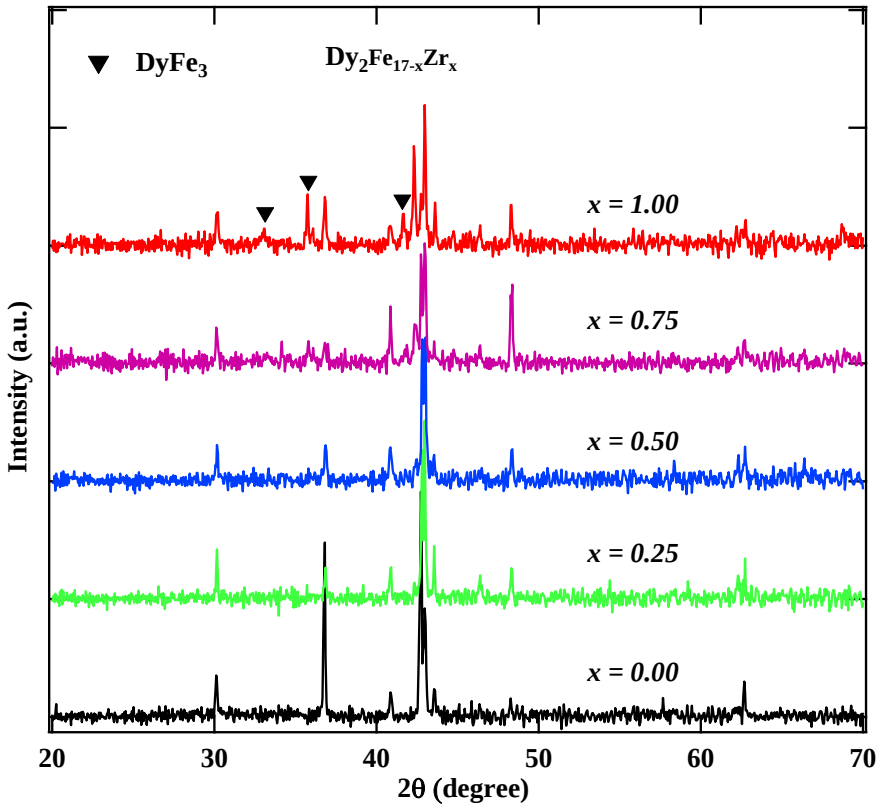

(a)

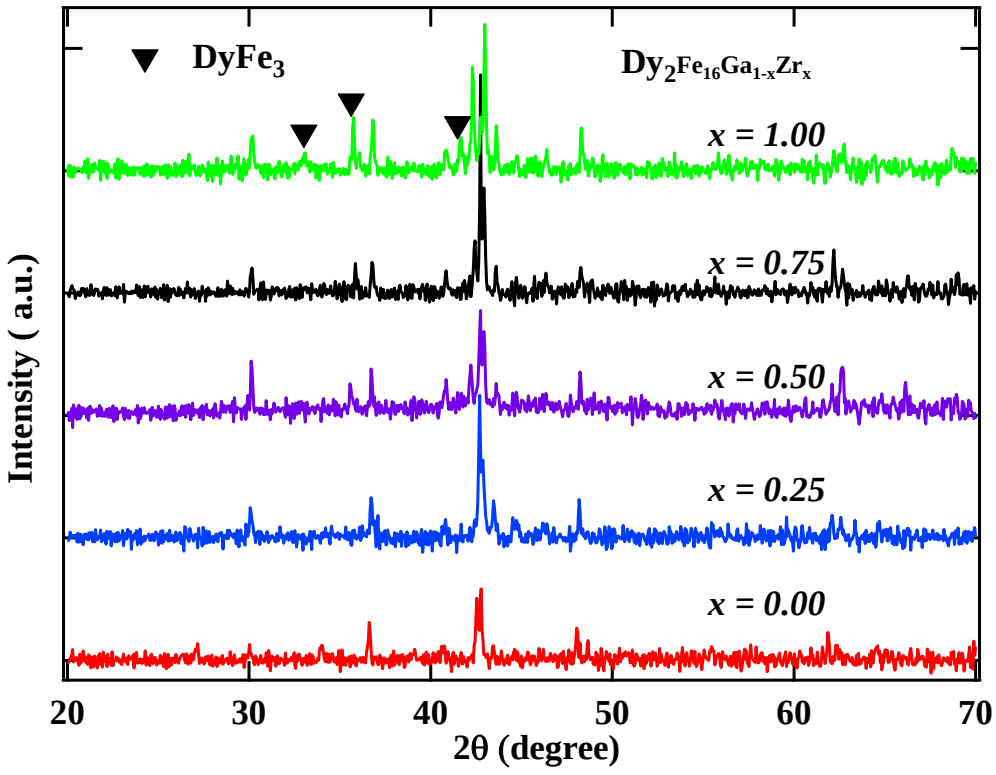

Preprints (www.preprints.org) | NOT PEER-REVIEWED | Posted: 17 July 2019 doi:10.20944/preprints201907.0206.v1

(**b**)

Figure 1. X-ray diffraction patterns of (a) $Dy_2Fe_{17-x}Zr_x$ (b) $Dy_2Fe_{16}Ga_{1-x}Zr_x$ compounds.

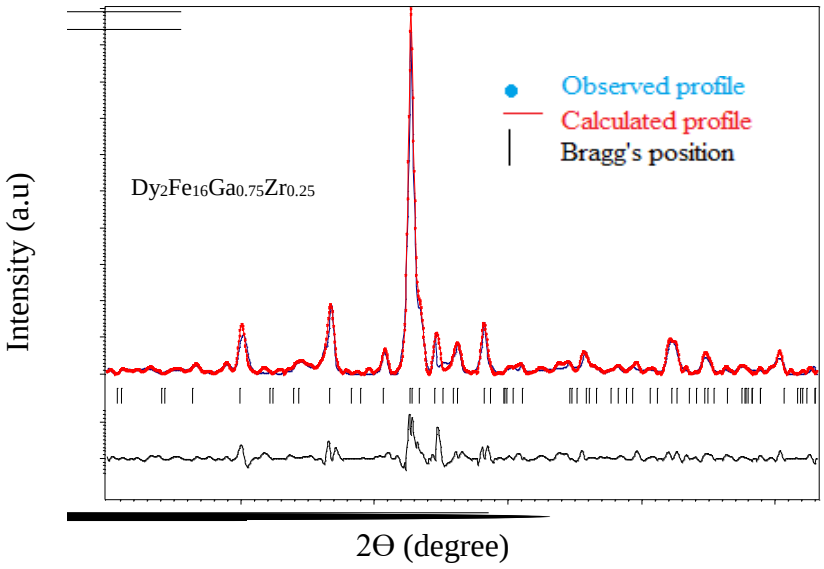

Figure 2. Rietveld refinement profile for $Dy_2Fe_{16}Ga_{0.75}Zr_{0.25}$

.

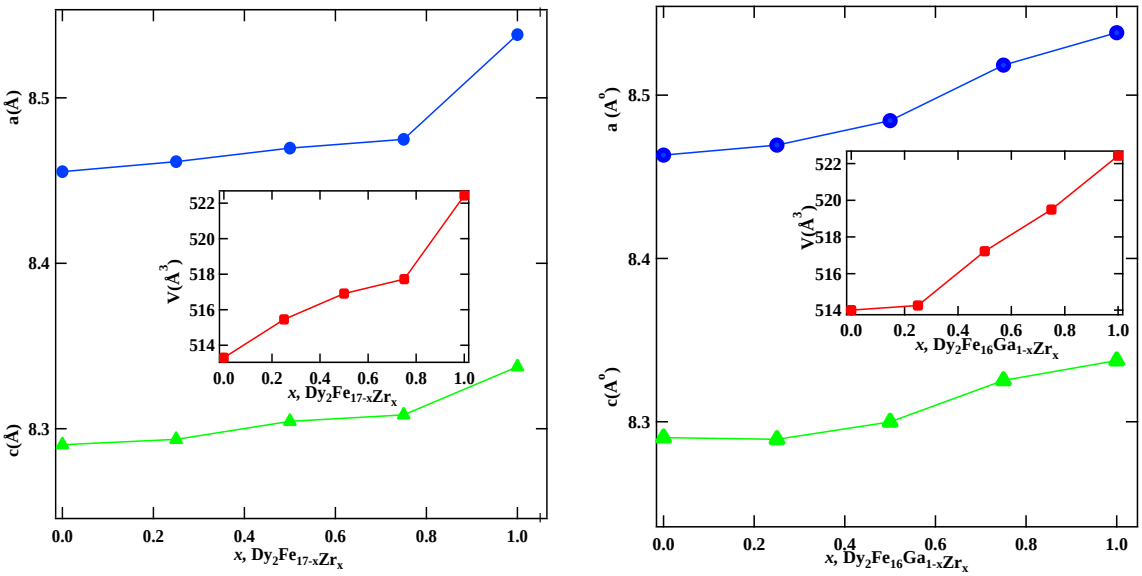

Preprints (www.preprints.org) | NOT PEER-REVIEWED | Posted: 17 July 2019 doi:10.20944/preprints201907.0206.v1

Figure 3. Lattice parameters *a* and *c* and unit cell volume of (a) $Dy_2Fe_{17-x}Zr_x$ and (b) $Dy_2Fe_{16}Ga_{1-x}Zr_x$ as a function of Zr content.

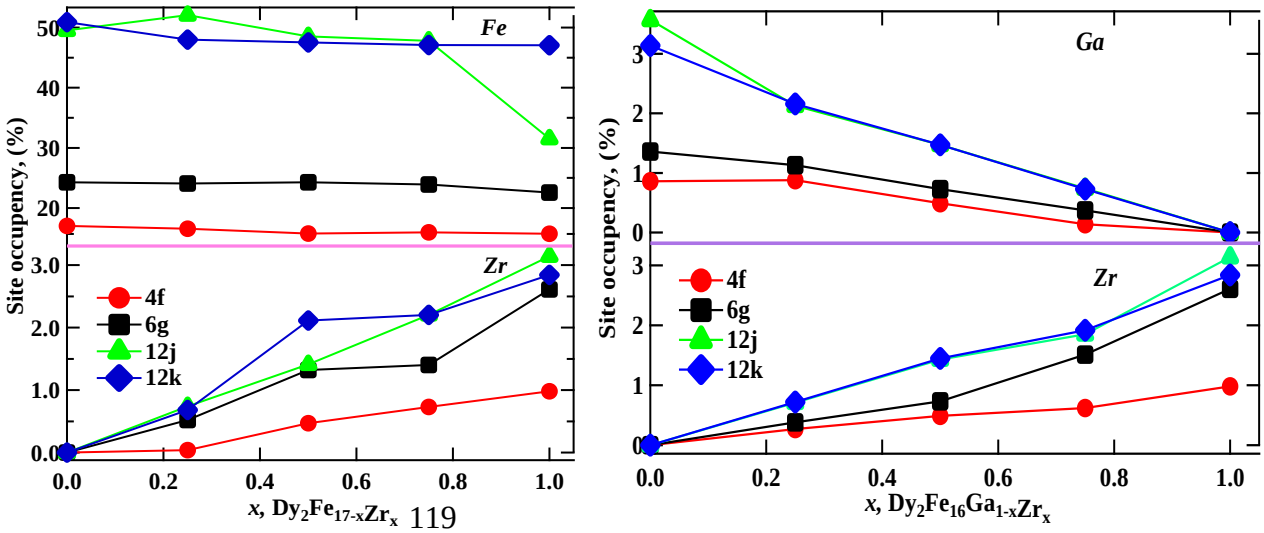

(a) (b)

Figure 4. The percentage occupancy of Fe and Zr at iron sites in (a) $Dy_2Fe_{17-x}Zr_x$ (b) Fe and Zr at Ga sites in $Dy_2Fe_{16}Ga_{1-x}Zr_x$ as a function of Zr content.

Preprints (www.preprints.org) | NOT PEER-REVIEWED | Posted: 17 July 2019 doi:10.20944/preprints201907.0206.v1

Table 1. Lattice parameters and unit cell volume of $Dy_2Fe_{17-x}Zr_x$ and $Dy_2Fe_{16}Ga_{1-x}Zr_x$ obtained from Rietveld refinements.

		a (Å)	c (Å)	V (Å^3)	R_{obs} (%)	wR_{obs} (%)	R_p (%)	wR_p (%)
$Dy_2Fe_{17-x}Zr_x$	0	8.45541(11)	8.29036(4)	513.303(18)	4.17	5.95	10.65	14.49
	0.25	8.46147(19)	8.29361(13)	515.456(21)	3.13	4.16	12.32	15.43
	0.5	8.46963(16)	8.30442(12)	516.913(16)	4.16	4.33	11.91	17.21
	0.75	8.4749(14)	8.30836(11)	517.725(21)	4.52	5.11	9.32	10.12
	1	8.53823(17)	8.33743(19)	522.429(13)	5.01	6.99	9.96	10.21
$Dy_2Fe_{16}Ga_{1-x}Zr_x$	0	8.46324(3)	8.29025(3)	514.013(26)	5.97	6.17	10.21	12.13
	0.25	8.46943(15)	8.28922(7)	514.265(28)	5.65	6.97	13.64	16.98
	0.5	8.48437(12)	8.29985(5)	517.221(23)	4.52	5.11	9.32	10.12
	0.75	8.51833(7)	8.32536(7)	519.498(13)	5.21	6.12	12.21	11.21
	1	8.53823(17)	8.33743(19)	522.429(13)	5.01	6.99	9.96	10.21

Table 2. The site occupancy table for $Dy_2Fe_{17-x}Zr_x$ and $Dy_2Fe_{16}Ga_{1-x}Zr_x$.

	x	Fe(4*f*)	Fe(6*g*)	Fe(12*j*)	Fe(12*k*)	Zr(4*f*)	Zr(6*g*)	Zr(12*j*)	Zr(12*k*)
Site occupancy for $Dy_2Fe_{17-x}Zr_x$ (%)	0.00	16.9(59)	24.3(6)	49.5(95)	50.9(31)	0	0	0	0
	0.25	16.5(2)	24.1(7)	52.0(1)	48.0(4)	0.04(3)	0.52(6)	0.74(1)	0.68(13)
	0.50	15.7(1)	24.3(4)	48.5(12)	47.5(7)	0.47(14)	1.32(15)	1.41(3)	2.11(17)
	0.75	15.9(2)	23.9(5)	47.7(1)	47.1(17)	0.73(8)	1.40(3)	2.20(6)	2.20(15)
	1.00	15.6(4)	22.6(4)	31.5(1)	47.0(3)	0.98(7)	2.61(6)	3.14(3)	2.84(11)
	x	Ga(4*f*)	Ga(6*g*)	Ga(12*j*)	Ga(12*k*)	Zr(4*f*)	Zr(6*g*)	Zr(12*j*)	Zr(12*k*)
Site occupancy for $Dy_2Fe_{16}Ga_{1-x}Zr_x$ (%)	0.00	0.86(21)	1.36(15)	3.57(16)	3.14(23)	0	0	0	0
	0.25	0.88(43)	1.13(43)	2.13(12)	2.16(11)	0.27(12)	0.38(14)	0.71(36)	0.72(41)
	0.50	0.49(31)	0.73(42)	1.47(13)	1.47(32)	0.49(41)	0.73(32)	1.43(32)	1.45(11)
	0.75	0.14(22)	0.37(62)	0.74(16)	0.73(31)	0.62(21)	1.51(21)	1.85(22)	1.92(13)
	1.00	0	0	0	0	0.98(7)	2.61(6)	3.14(3)	2.84(11)

Preprints (www.preprints.org) | NOT PEER-REVIEWED | Posted: 17 July 2019 doi:10.20944/preprints201907.0206.v1

Table 3 represents the distance between the Fe-Fe neighbor sites, Ms and Tc for $Dy_2Fe_{17-x}Zr_x$ and $Dy_2Fe_{16}Ga_{1-x}Zr_x$ and the values are plotted in **Figure 5(a)** and **(b)**. It can be observed from **Table 3** that the average bond distance between each site changes with the concentration of both Zr and Ga (4*f*-4*f* ~2.42 Å), (12*k*-12*k* ~ 2.46 Å) and (12*j*-12*j* ~ 2.52 Å). *12j-12j* sites show both Zr and Ga prefers to stay in the same sites.

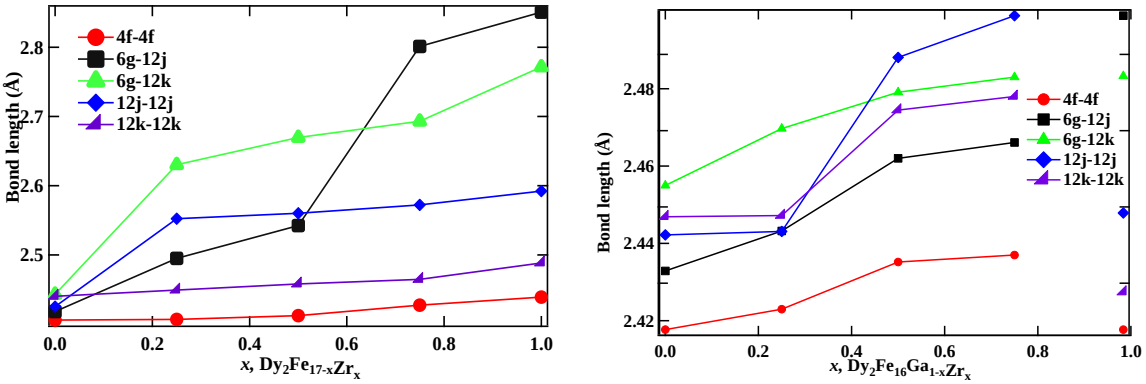

Figure 5. Dependence of bond lengths on *x* of (a) $Dy_2Fe_{17-x}Zr_x$ (b) $Dy_2Fe_{16}Ga_{1-x}Zr_x$.

Table 3. Distance between the Fe-Fe neighbor sites, Ms and Tc for $Dy_2Fe_{17-x}Zr_x$ and $Dy_2Fe_{16}Ga_{1-x}Zr_x$.

x	Bond length $Dy_2Fe_{17-x}Zr_x$(Å)					Bond length $Dy_2Fe_{16}Ga_{1-x}Zr_x$ (Å)				$Dy_2Fe_{17-x}Zr_x$		$Dy_2Fe_{16}Ga_{1-x}Zr_x$	
	4*f*-4*f*	6*g*-12*j*	6*g*-12*k*	12*j*-12*j*	12*k*-12*k*	4*f*-4*f*	6*g*-12*j*	6*g*-12*k*	12*j*-12*j*	Ms (emu/g)	Tc (K)	Ms	Tc (K)
0.00	2.406	2.418	2.443	2.425	2.44	2.418	2.433	2.455	2.442	62.94	408	61.58	488
0.25	2.407	2.495	2.63	2.552	2.449	2.423	2.443	2.469	2.443	60.78	456	60.48	500.1
0.50	2.412	2.542	2.669	2.56	2.458	2.435	2.462	2.479	2.488	58.57	503.9	57.25	505.1
0.75	2.427	2.801	2.693	2.572	2.464	2.437	2.466	2.483	2.499	55.04	510	56.39	502.5
1.00	2.439	2.851	2.772	2.592	2.488	2.439	2.85	2.771	2.592	52.07	425	52.07	425

The room temperature magnetic properties obtained from M vs. H measurement for $Dy_2Fe_{17-x}Zr_x$ and $Dy_2Fe_{16}Ga_{1-x}Zr_x$ are plotted in **Figure 6(a)** and **(b)** respectively. The M vs. H plot shows that the saturation magnetization (Ms) decreases with an increase in the Zr substitution in both $Dy_2Fe_{17-x}Zr_x$ and $Dy_2Fe_{16}Ga_{1-x}Zr_x$. The "Law of Approach" to saturation magnetization was used to determine the saturation magnetization, *Ms*. The "Law of approach" describes the relationship between magnetization M on the applied magnetic field for H greater than coercive field *Hc*. The magnetization near *Ms* can be written as $M = Ms\left(1-\frac{a}{H}-\frac{b}{H^2}\right)+\kappa H$ [32] where *M* is the magnetization, *H* is the applied magnetic field, and *Ms* is the saturation magnetization attained at high field. The term κH represents the field-induced increase in the spontaneous magnetization of the domains. This term is very small at a temperature well below the Curie temperature and could be neglected. The term "*a*" is generally interpreted as due to microstress and ignored in the high field region, and "*b*" as due to crystal anisotropy. Where magneto-crystalline is a dominant term, a plot of *M* vs. $1/H^2$ in the high field region gives a straight line, the intercept of which (with the *M*-axis) gives the *Ms* and the slope of which gives the magneto-crystalline anisotropy constant. An interesting variation in *Ms* is noticed with the Zr atom doping. The decrease in saturation magnetization in $Dy_2Fe_{17-x}Zr_x$ with the increase in Zr content is attributed to the substitution of non-magnetic Zr atom for Fe atom. This decrease in the saturation magnetization is the result of the dilution effect *i.e.* replacing Fe atom (2.2 μ_B) with non-magnetic Zr atom. Similar reduction in Ms has been reported earlier for $Dy_2Fe_{17-x}Ga_x$ [18], $Ce_2Fe_{17-x}Ga_x$ [33], $Sm_2Fe_{17-x}Ga_x$ [34] compounds. From **Figure 6(c)**, it is observed that the saturation magnetization decreases linearly from 62.94emu/g to 52.07emu/g per Zr atom for $Dy_2Fe_{17-x}Zr_x$ however magnetization decreases from 61.58emu/g to 52.07emu/g in $Dy_2Fe_{16}Ga_{1-x}Zr_x$. The dropdown of magnetization in both cases could be due to the reduction of the magnetic moment of iron by Zr atoms.

Preprints (www.preprints.org) | NOT PEER-REVIEWED | Posted: 17 July 2019 doi:10.20944/preprints201907.0206.v1

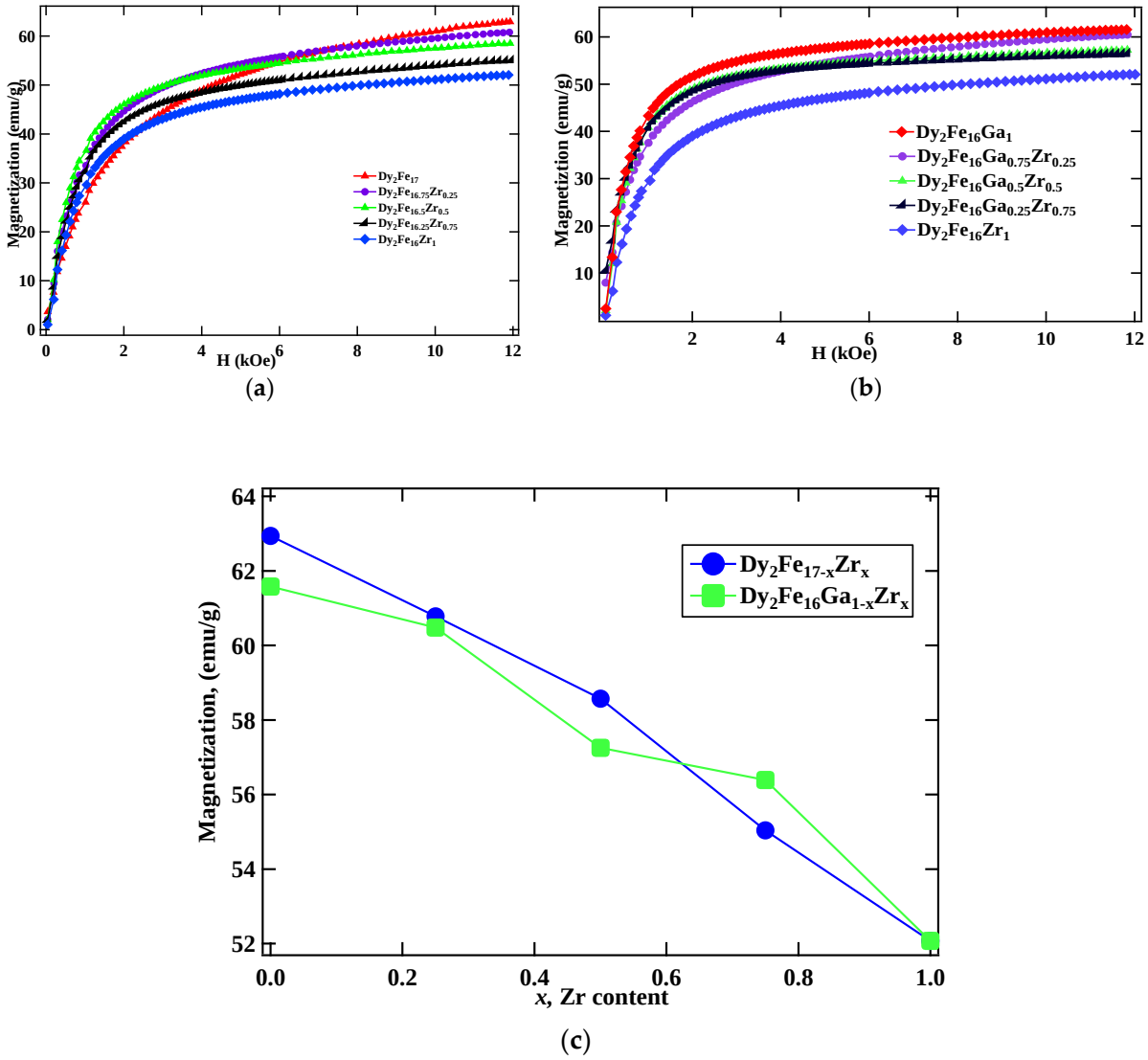

Figure 6. RT M vs. H plot of (a) $Dy_2Fe_{17-x}Zr_x$ (b) $Dy_2Fe_{16}Ga_{1-x}Zr_x$ (**c**) Magnetization (Ms) vs. *x* for $Dy_2Fe_{17-x}Zr_x$ and $Dy_2Fe_{16}Ga_{1-x}Zr_x$.

The Curie Temperature (Tc) of $Dy_2Fe_{17-x}Zr_x$ and $Dy_2Fe_{16}Ga_{1--x}Zr_x$ as a function of Zr content is shown in **Figure 7** and corresponding data are listed in **Table 3**. It is observed that for $Dy_2Fe_{17-x}Zr_x$ Curie temperature increases from 408 K ($x = 0.00$) to a maximum of 510 K ($x = 0.75$) and then decreases to 425 K ($x = 1.00$). The achieved curie temperature of $Dy_2Fe_{16.25}Zr_{0.75}$ is 102 K higher than that of Dy_2Fe_{17}. It is observed from **Figure 5(a) and (b)** that the bond length increases with the increase in the Zr content. In general, the curie temperature in rare-earth intermetallic is due to three kinds of exchange interactions namely the 3d-3d exchange interactions *i.e.* between the magnetic moment of the Fe sub-lattice (J_{FeFe}), 4f-4f exchange interaction i.e. the interaction between the magnetic moment within the R sub-lattice (J_{RR}), and the inter sub-lattice 3d-4f exchange interaction (J_{RFe}). It is reported that the Curie temperature (Tc) increases with an increase in the J_{FeFe} [35]. Thus, the increase or decrease in Tc in the R_2Fe_{17} intermetallic may be due to the increase or decrease in the interaction

Preprints (www.preprints.org) | NOT PEER-REVIEWED | Posted: 17 July 2019 doi:10.20944/preprints201907.0206.v1

parameter J_{FeFe}. The interactions between the rare-earth spins (4f-4f) are assumed to be weak and negligible in comparison with the other two types of interactions. The low Tc observed in parent Dy_2Fe_{17} compound is believed to be due to the short Fe–Fe interatomic distances found at the 4f(6c) sites in the hexagonal (rhombohedral) structure which couple antiferromagnetically [36] since their separation is less than 2.45 Å **Figure 5(a)** and **(b)**, needed for ferromagnetic ordering [37]. In the compounds with hexagonal structure the Fe(4f)- Fe(4f) interactions are strongly negative whereas the Fe(6g)- Fe(12j), Fe(6g)-Fe(12k) and Fe(12k)-Fe(12k) interactions are weakly negatives. Thus, the increase in Tc is considered due to the increase in strength of the Fe-Fe exchange coupling that occurs from the increase in Fe-Fe bond lengths for Fe-reach R_2Fe_{17} compounds. The strength of Fe-Fe exchange interaction highly depends on interatomic Fe-Fe distance [38,39]. Accordingly, the exchange interactions between iron atoms situated at distances smaller (greater) than 2.45−2.50 Å are negative (positive). In the R_2Fe_{17} majority of Fe-Fe distances favor the negative interaction [18]. The negative exchange interaction can be reduced either by volume expansion or by reducing the number of Fe-Fe pairs with negative exchange interactions. It is noted that the increase in Tc has been reported earlier with Ga substitution (x=1) [18] however with the simultaneous substation of non-magnetic Ga and Zr atoms enhances the curie temperature of the intermetallic that we have reported without significantly lowering the saturation magnetization. It is found that, for $Dy_2Fe_{16}Ga_{1-x}Zr_x$, Curie temperature increases slowly from 488 K (x = 0.00) to maximum of 505.1 K (x = 0.50) and then decreases to 425 K (x = 1.00). The maximum Tc observed in $Dy_2Fe_{16}Ga_{0.5}Zr_{0.5}$ (505.1 K) is 17.1 K greater than of $Dy_2Fe_{16}Ga_1$ and 97 K higher than the Dy_2Fe_{17} which is indicating that double substitution of Zr and Ga does slow enhancement in Tc over the single substation.

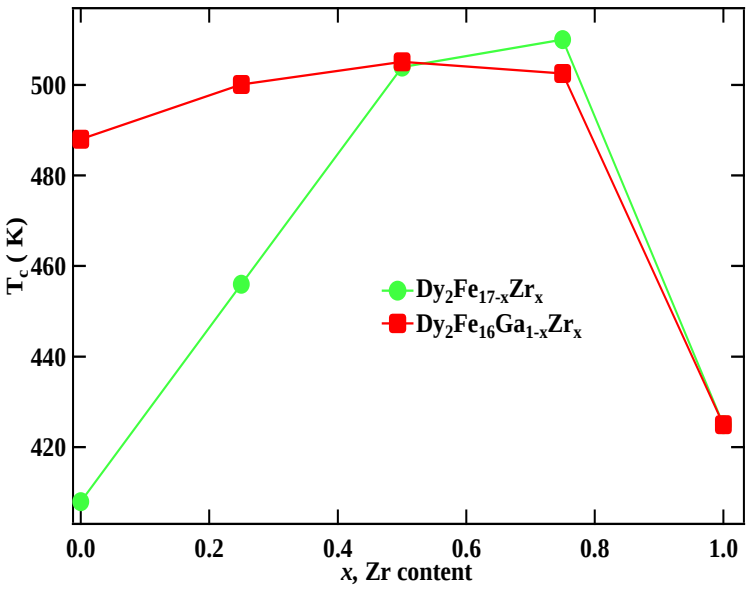

Figure 7. Comparative study for the Tc vs. x for $Dy_2Fe_{17-x}Zr_x$ and $Dy_2Fe_{16}Ga_{1-x}Zr_x$.

The Mössbauer spectra are plotted in **Figure 8(a) and (b)** for $Dy_2Fe_{17-x}Zr_x$ and $Dy_2Fe_{16}Ga_{1-x}Zr_x$ (x=0.00, 0.25, 0.50, 0.75, 1.00) respectively. The resulting spectra were fitted using the WMOSS program. Since the Dy_2Fe_{17} compounds have a basal magnetization, either seven or eight magnetic sextets are required to fit their Mössbauer spectra. The fitted data are shown in **Fig. 8(a)** and **(b)** was carried out with eight magnetic sextets assigned to 4*f*, 6*g*, 12*j*, and 12*k* sites in Dy_2Fe_{17}. Doublets were used for additional phases for the sample at x=1 for the paramagnetic phase ($DyFe_3$) observed during Mössbauer fitting.

 doi:10.20944/preprints201907.0206.v1

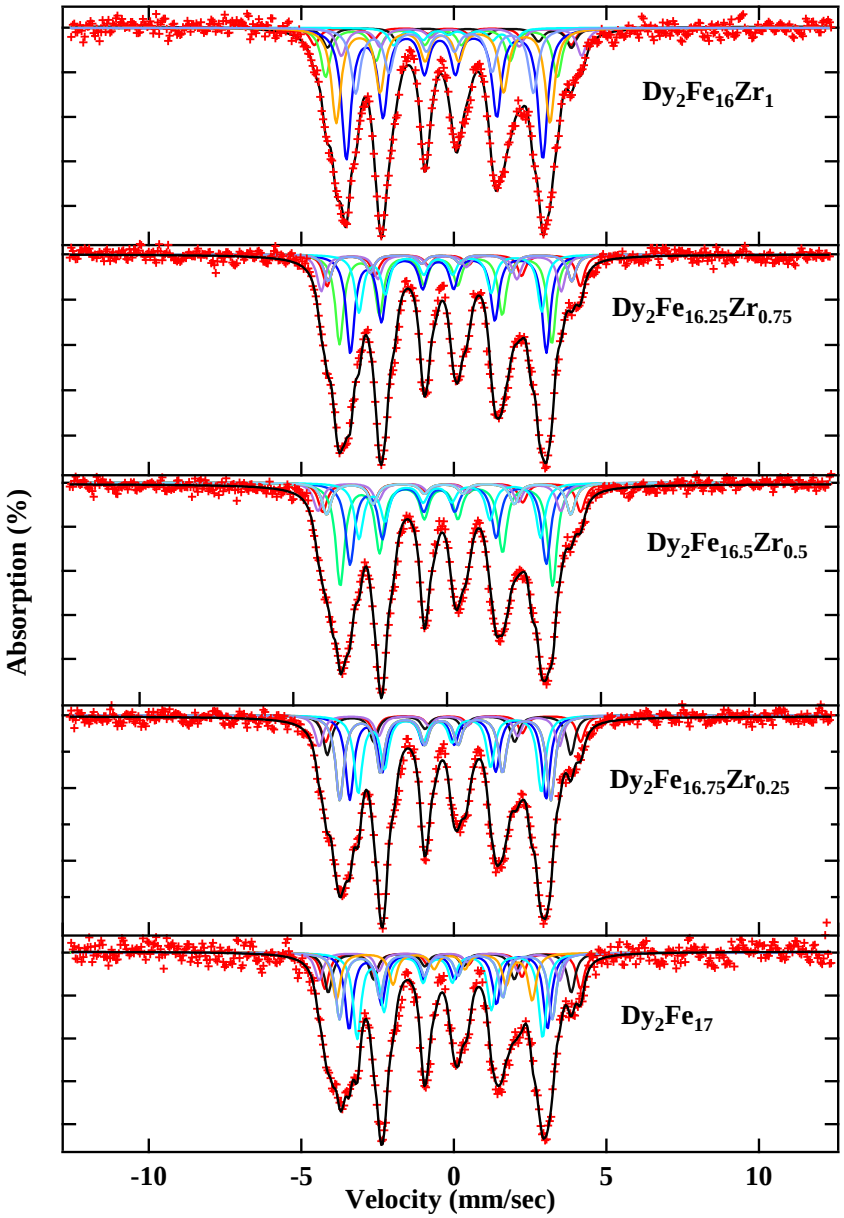

(a)

Preprints (www.preprints.org) | NOT PEER-REVIEWED | Posted: 17 July 2019 doi:10.20944/preprints201907.0206.v1

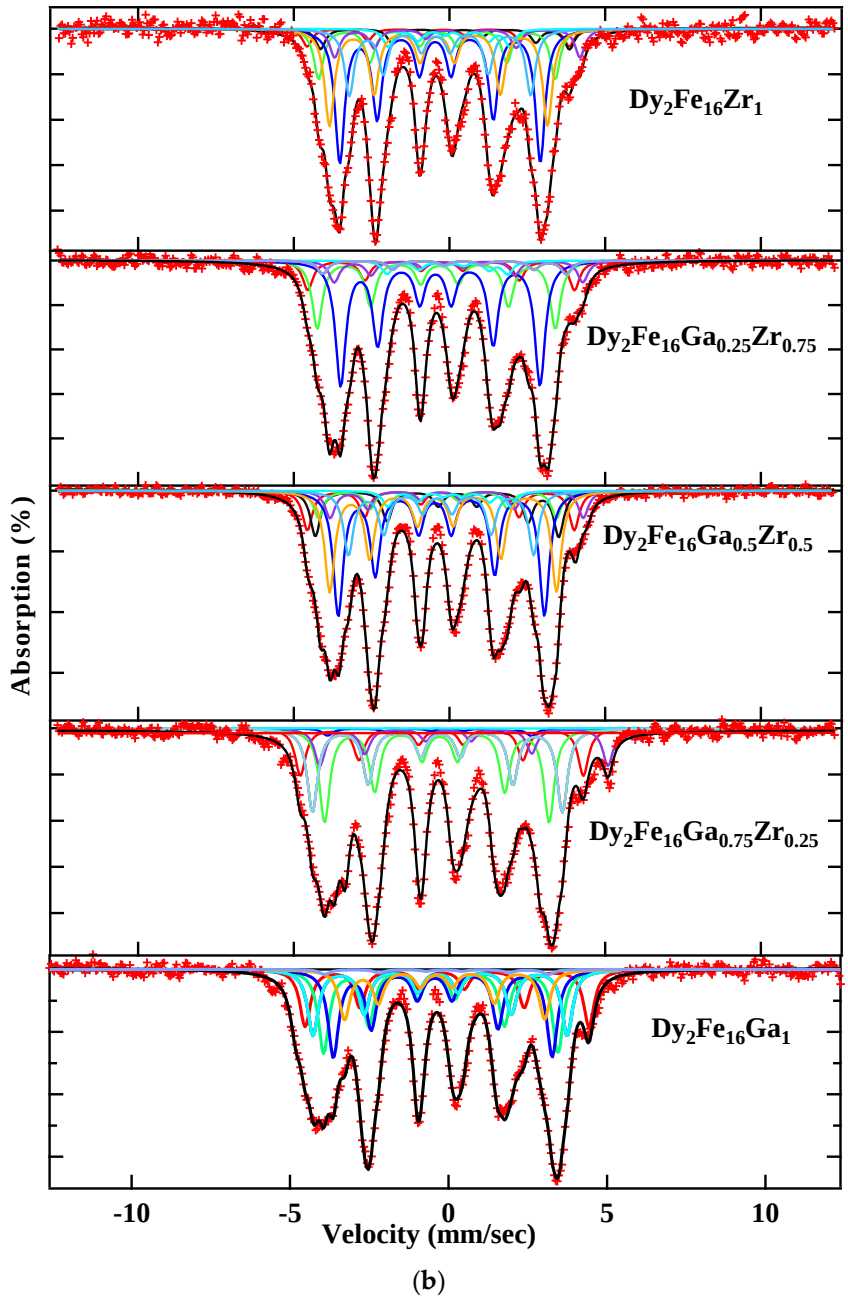

Figure 8. RT Mössbauer spectra for (a) $Dy_2Fe_{17-x}Zr_x$ (b) $Dy_2Fe_{16}Ga_{1-x}Zr_x$.

The hyperfine parameters derived from the fitting are listed in **Table 4(a)** and **(b)** and the hyperfine field (HF) and isomer shifts (IS) are plotted in **Figure 9(a)** and **(b)**. There exists a direct correlation between hyperfine field values of a site to its near neighbor (NN) iron sites. In case of Th_2Ni_{17} structure, 12*k* site has 9 NN Fe sites (1 (4*f*), 2 (6*g*), 4 (12*j*), 2(12*k*)), *12j* has 10 NN Fe sites (2 (4*f*), 2 (6*g*), 2 (12*j*), 4 (12*k*)), 6*g* has 10 NN Fe sites (2 (4*f*), 0 (6*g*), 4 (12*j*), 4(12*k*)), and 4*f* site has 11 NN Fe sites (1 (4*f*), 3 (6*g*), 6 (12*j*), 3 (12*k*)). Following the NN distribution, the observed HF values are in 4*f*(6*c*)>12*j*(18*f*)>6*g*(9*d*)>12*k*(18*h*) sequence, which is similar to the sequence observed in other R_2Fe_{17} compounds [40,41]. It is obvious that 4*f* (6*c*) site has the maximum hyperfine field, since it has the maximum number of Fe nearest neighbors, whereas, the 18*h* (12*k*) site has the minimum number of Fe neighbors and consequently has the least HF value. Although 6*g*(9*d*) and 12*j*(18*f*) sites have the same number of Fe neighbors, the former has comparatively smaller Fe-Fe distances and hence a larger hyperfine field. The hyperfine field (B_{hf}) decreases with increasing Zr content. The decrease in the hyperfine fields could be from the decrease in magnetic moments of iron in $Dy_2Fe_{17-x}Zr_x$. It is found that the 9.23% of total area occupied by the $DyFe_3$ paramagnetic phase for x = 1 Zr content.

Preprints (www.preprints.org) | NOT PEER-REVIEWED | Posted: 17 July 2019 doi:10.20944/preprints201907.0206.v1

This observation supports the formation of additional paramagnetic phase $DyFe_3$ as seen in the XRD plot in **Figure 1.**

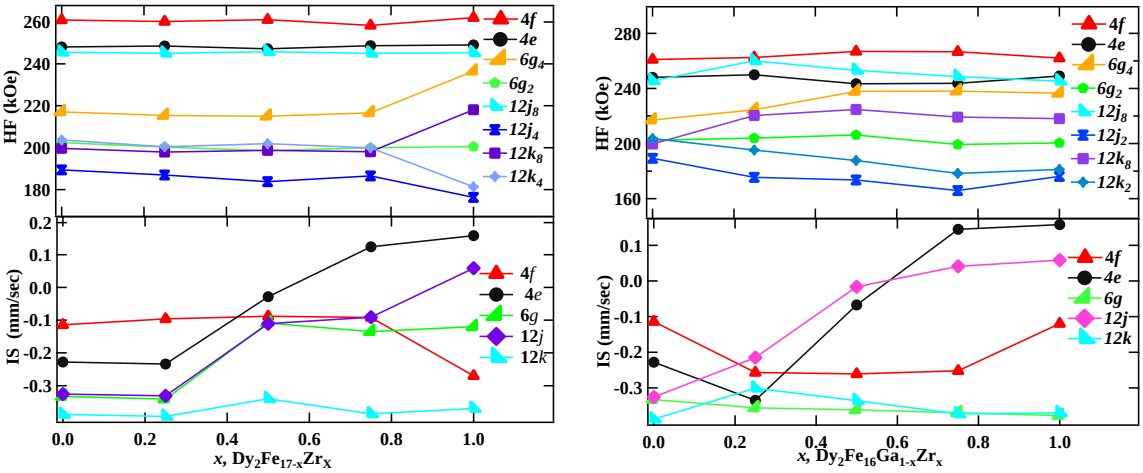

Figure 9. RT Mössbauer hyperfine parameters plots for (a) $Dy_2Fe_{17-x}Zr_x$ (b) $Dy_2Fe_{16}Ga_{1-x}Zr_x$.

Table 4. (a) The RT hyperfine parameters, HF (kOe), IS (mm/sec), QS (mm/sec) and area (%) of the $Dy_2Fe_{17-x}Zr_x$.

	x	4*f*	4*e*	6g_4	6g_2	12j_8	12j_4	12k_8	12k_4	Doublet
HF (kOe)	0.00	261.0	248.0	217.0	202.4	245.6	189.0	199.7	203.7	
	0.25	260.2	248.5	215.3	200.3	245.0	187.0	197.9	200.4	
	0.50	261.1	247.1	214.9	198.6	245.8	184.0	198.7	201.9	
	0.75	258.4	248.7	216.6	200.0	245.0	186.0	198.0	199.9	
	1.00	262.1	249.0	236.5	200.5	245.3	176.0	218.1	181.3	34.0
IS (mm/s)	0.00	-0.114	-0.228	-0.333	-0.33	-0.326	-0.33	-0.39	-0.39	
	0.25	-0.096	-0.234	-0.341	-0.34	-0.331	-0.33	-0.39	-0.39	
	0.50	-0.088	-0.028	-0.109	-0.11	-0.111	-0.11	-0.34	-0.34	
	0.75	-0.092	0.124	-0.135	-0.14	-0.091	-0.09	-0.39	-0.39	
	1.00	-0.27	0.158	-0.12	-0.12	0.059	0.06	-0.37	-0.37	0.056
QS (mm/s)	0.00	0.152	0.191	0.152	0.303	-0.295	0.4	0.083	-0.58	
	0.25	0.152	0.16	0.128	0.296	-0.291	0.4	-0.03	-0.58	
	0.50	0.119	0.163	0.175	0.289	-0.276	0.4	0.121	-0.5	
	0.75	0.178	0.301	0.157	0.335	-0.199	0.4	-0.03	-0.58	
	1.00	0.123	0.25	-0.048	0.155	-0.25	0.35	0.042	-0.58	-0.39
Area (%)	0.00	4.0	1.91	15.3	17.5	4.3	19.5	10.9	13.1	
	0.25	5.5	8.2	17.7	17.4	6.3	16.0	10.4	13.3	
	0.50	6.2	6.7	21.9	17.3	6.0	11..7	9.60	15.1	
	0.75	5.25	4.0	21.0	19.0	7.6	14.0	14.81	13.5	
	1.00	4.2	4.9	11.2	31.9	6.2	4.21	23.1	15.2	9. 23

Preprints (www.preprints.org) | NOT PEER-REVIEWED | Posted: 17 July 2019 doi:10.20944/preprints201907.0206.v1

Table 4. (b) The RT hyperfine parameters, HF (kOe), IS (mm/sec), QS (mm/sec) and area (%) of the $Dy_2Fe_{16}Ga_{1-x}Zr_x$.

	x	4*f*	4*e*	6g_4	6g_2	12j_8	12j_4	12k_8	12k_4	Doublet
HF (kOe)	0.000	278.7	249.7	230.2	214.9	260	218.2	196.5	220	
	0.25	282.9	249.9	224.5	204	288.1	164.8	220.3	195.3	
	0.5	267.6	267.9	229	204	254.2	123.4	226.8	185.3	
	0.75	266.7	243.7	238.1	199.4	248.6	120.7	219.2	178.3	
	1.00	262.1	248.9	236.5	200.4	245.3	122	218.1	181.3	34
IS (mm/s)	0.00	-0.126	-0.301	-0.309	-0.309	-0.422	-0.422	-0.254	-0.254	
	0.25	-0.257	-0.335	-0.356	-0.356	0.215	0.215	-0.301	-0.301	
	0.50	-0.227	-0.509	-0.367	-0.367	0.068	0.068	-0.327	-0.327	
	0.75	-0.252	0.145	-0.37	-0.37	0.041	0.041	-0.373	-0.373	
	1.00	-0.27	0.158	-0.378	-0.378	0.058	0.058	-0.37	-0.37	0.0557
QD (mm/s)	0.00	0.158	0.0107	0.133	0.259	-0.418	-0.48	0.259	-0.58	
	0.25	0.084	-0.102	-0.093	-0.568	0.5	-0.477	0.284	0.178	
	0.50	-0.069	-0.7	-0.196	0.201	0.5	-0.134	0.249	0.118	
	0.75	-0.029	-0.6	-0.102	0.156	0.5	-0.214	0.057	0.079	
	1.00	-0.181	-0.6	-0.049	0.155	0.39	-0.142	0.042	0.136	-0.388
Area (%)	0.00	13.7	15.9	20	21	10.5	5.5	11.9	3.9	
	0.25	5.2	16.7	18.8	4.62	5.5	2.6	19	20.2	
	0.50	7.4	7.8	18.7	17.73	6.17	5.5	22.1	14.1	
	0.75	6.75	3.8	28.2	4.3	3	26.8	12	14.4	
	1.00	4.2	4.87	11.2	31.9	6.16	4.2	23.1	15.2	9. 23

On average, the isomer shifts (IS) of all sites increases with the increase in Zr content. The increase in the isomer shift (IS) could be related to the volume expansion resulting from the Zr substitution for Fe. The volume expansion lowers the *s*-electron density at the Fe nuclei which leads to an increase in isomer shift (IS). At higher Zr content (x = 1.00), a decrease in isomer shift (IS) was observed. This decrease in the isomer shift may be due to the combined effect of volume expansion and the increase in electron density. The decrease in hyperfine fields on $Dy_2Fe_{16}Ga_{1-x}Zr_x$ is attributed due to the decrease in magnetization because of the competition between the positive effect on magnetic moments due to bond length and the negative effect caused by magnetic dilution of the substituted non-magnetic atom. The average isomer shift (IS) of all sites increases with increasing Zr content except the 12*k* site. The increase in the isomer shift (IS) could be related to the volume expansion resulting from the Zr substitution for Ga. The volume expansion lowers the electron density at the Fe nuclei which leads to an increase in isomer shift (IS).

4. Conclusions

The effect of substitution of Ga and Zr in intermetallic compounds Dy_2Fe_{17} prepared via arc melting are carefully studied. The intermetallic compounds are α-Fe free and are found to crystallize in hexagonal Th_2Ni_{17} type structure. Paramagnetic phase $DyFe_3$ is observed for x=1 and confirmed using Mössbauer spectroscopy. From the Rietveld refinement, it is observed that most of Zr atoms occupying 12*j* and 12*k* sites of Fe for $Dy_2Fe_{17-x}Zr_x$ and $Dy_2Fe_{16}Ga_{1-x}Zr_x$ intermetallic compound. Lattice parameters *a, c* and unit cell volume are increasing with the substitution of Zr and Ga. The Fe-Fe bond length increases with Zr substitution. However, the maximum change in Fe-Fe bond length is observed for 6*g*-12*j*, 6*g*-12*k* and 12*j*-12*j* sites. This change in bond length found to be affected by the strength of Fe-Fe exchange interaction. The maximum Tc is observed in $Dy_2Fe_{16}Ga_{0.5}Zr_{0.5}$ (505.1 K) for double substitution of Ga and Zr however for single substitution, maximum Tc is observed as 510K in $Dy_2Fe_{16.25}Zr_{0.75}$. This indicates that double substitution of Zr and Ga does slow enhancement in Tc with the single substitution. Ga and Zr dopant and their content can significantly improve Tc and Ms thus ensuring their potential use in high-temperature permanent magnet applications. The hyperfine field values decrease for both $Dy_2Fe_{17-x}Zr_x$ and $Dy_2Fe_{16}Ga_{1-x}Zr_x$ with Zr doping due to the decrease in

the magnetic moment of Fe atoms. The isomer shift (IS) showed an increase in nature due to the increase in volume effect.

Acknowledgment: The authors would like to acknowledge NSF-CMMI (Grant #: 1029780) and NSF-TN-SCORE (Grant #:EPS-10004083) for financially supporting this work.

Conflict of Interest: The authors declare no conflict of interest.

References

1. K. J. Strnat, "Chapter 2 – Rare-earth-cobalt permanent magnets," in *Handbook of Ferromagnetic Materials*, vol. **4**, p. 131–209 (1988).
2. H Oesterreicher, D. McNeely "Studies on compounds $DyFe_3$, Dy_6Fe_{23} and Dy_2Fe_{17} with al substitution for Fe I: structural investigations" *J. less comm Metals*, 53 2 235-243 (1977)
3. J. Pszczola, J. Zukrowski, J. Suwalski, Z. Kucharski, M. Lukasiak "The ^{161}Dy and ^{57}Fe Mössbauer studies of the $Dy_2Fe_{17-y}Al_y$compounds" *J. Magn. Magn. Mater*, 40 1, 197 (1983)
4. R. Pfranger, D. Plusa, S. Szymura, B. Wyslocki "Domain Structures and anisotropy constant in the compound Dy_2Fe_{17}" *J. Magn.Mag. Mater*. 21 1 43 (1980)
5. K.V.S Rama Rao, H. Ehrenberg, G. Markandeyulu, U.V. Varadaraju, M. Venkatesan, K.G. Suresh ,V.S. Murthy, P.C. Schmidt, H. Fuess, "On the Structural and Magnetic Properties of $R_2Fe_{17-x}(A,T)_x$ (R = Rare-Earth; A = Al, Si, Ga; T = Transition Metal) Compounds" *J. phys. Stat. sol. (a)* 189, 2, 373 (2002)
6. N. Plugaru, J. Rubin, J. Bartolome, C. Piquer, M. Artigas, "Magnetic properties of $RFe_{11.3}W_{0.7}$ (R=Dy, Ho, Er, and Lu): On the R−Fe exchange interaction in the R(Fe,T)12 class of compounds", *Phys. Review B*, 65 134419 (2002).
7. M. Zinkevich, N. Mattern, I. Bacher and S. Puerta, "Formation, crystal structure and magnetic properties of (1:12) compounds in the Fe-Gd-Mo-Zr system," *J. Alloys and compounds*, vol. **336**, pp. 320-328, 2002
8. Z. Chen, G.C. Hadjipanayis "Effects of Cr substitution on the formation, structure and magnetic properties of Sm $_2(Fe,Cr)_{17}C_x$ alloys" *IEEE Transactions on Magnetics* **33**, 5 , 3856-3858 (1997)
9. M.Kataoka,T. Satoh, and E. Otsuki. "Structure and magnetic properties of Sm_3 (Fe, V) $_{29}$ N_x." *Journal of applied physics* **85,** 8, 4675-4677 (1999).
10. B. Gebel, M. Kubis, and K-H. Müller. "Permanent magnets prepared from $Sm_{10.5}Fe_{88.5}Zr_{1.0}N_y$ without homogenization." *J. of magn and magn mater.* 174.1-2 (1997).
11. J. N. Dahal, K.S. Ali, S.R. Mishra, and J. Alam. "Structural, Magnetic, and Mössbauer Studies of Transition Metal-Doped $Gd_2Fe_{16}Ga_{0.5}TM_{0.5}$ Intermetallic Compounds (TM= Cr, Mn, Co, Ni, Cu, and Zn)." *Magnetochemistry* vol. **4**, no. 4 (2018): 54.
12. J. M. D. Coey and Hong Sun, "Improved magnetic properties by treatment of iron-based rare earth intermetallic compounds in ammonia", J. Magn. Magn. Mater. **87**, L251, (1990).
13. J. M. D. Coey, Hong Sun, Y. Otani, and D. P. F. Hurley, "Gas-phase carbonation of R_2Fe_{17}; R = Y, Sm", *J. Magn. Magn. Mater*. **98**, 76 (1991).
14. X. P. Zhong, R. J. Radwanski, F. R. de B-er, T. H. Jacobs, and K. H. J. Buschow," Magnetic and crystallographic characteristics of rare-earth ternary carbides derived from R_2Fe_{17} compounds", *J. Magn. Magn. Mater*. **86**, 333 (1990).
15. K. H. J. Buschow, R. Coehoorn, D. B. de Mooji. K. de Waard, and T. H. Jacobs, "Structure and magnetic properties of $R_2Fe_{17}N_x$ compounds", *J. Magn. Magn. Mater*. **92**, L35 (1990).
16. Z Wang and R A Dunlap "Effects of Al substitutions on the magnetic anisotropy of Sm_2Fe_{17} compounds" *J. Phys. Condens. Matter*, **5** 1407-1414 (1993)
17. W. B. Yelon and H. XieNeutron diffraction and Mössbauer effect study of several $Nd_2Fe_{17-x}Al_x$ solid solutions, *J. Applied phys*., 73, 6029 (1993)
18. B.-g. Shen, Z.-h. Cheng, H.-y. Gong, B. Liang, Q.-w. Yan and W.-s. Zhan, "Magnetic anisotropy of $Dy_2Fe_{17-x}Ga_x$ compounds," *Solid State Communications*, vol. **95**, no. 11, pp. 813-816, 1995.
19. J. Coey and H. Sun, "Improved magnetic properties by treatment of iron-based rare-earth intermetallic compounds in amonia," *J. Mag. Magn. Mater.*, vol. **87**, no. 3, p. L251–L254, July 1990.
20. P. M. Gubbens, A. A. Moolenaar, G. J. Boender, A. M. v. d. Kraan, T. H. Jacobs and K. H. J. Buschow, "^{166}Er and ^{57}Fe Mössbauer effect in $Er_2Fe_{17}N_x$," *J. Mag. Magn. Mater.*, vol. **97**, no. 1-3, pp. 69-72, June 1991.

21. I. Betancourt and H. Davies, "Influence of Zr and Nb dopant additions on the microstructure and magnetic properties of nanocomposite $RE_2(Fe,Co)_{14}B/\alpha(Fe,Co)$ (RE=Nd–Pr) alloys," *J. Mag. Magn. Mater.*, vol. **261**, no. 3, p. 328–336, May 2003.
22. G. J. Long, G. K. Marasinghe, S. Mishra, O. A. Pringle, Z. Hu, W. B. Yelon, D. P. Middleton, K. H. J. Buschow and F. Grandjean, "A Magnetic, Neutron Diffraction, and Mössbauer Spectral Study of the $Nd_2Fe_{17-x}Al_x$ Solid Solutions," *J. Appl. Phys.*, vol. **76**, no. 9, pp. 5383-5384, 1994.
23. O. Isnard, S. Miraglia, J. L. Soubeyroux and D. Fruchart, "Neutron powder diffraction study of $R_2Fe_{17}H_x$ compounds with R = Pr and Nd," *Solid State Communications,* vol. **81**, no. 1, pp. 13-19, 1992.
24. J. M. D. Coey, "New permanent magnets; manganese compounds" J. Phys.: *Condens. Matter*, 26, 064211 (2014).
25. H. M. Rietveld, "A profile refinement method for nuclear and magnetic structures" *J. Appl. Cryst*. 2, 65 (1969).
26. V. Petříček, M. Dušek and L. Palatinus, "Crystallographic Computing System JANA2006: *General features*, Z. Kristallogr. **229**, 345 (2014).
27. L. X. Liao, Z. Altounican, and D. H. Ryan, "Cobalt site preferences in iron rare-earth-based compounds," *Phy. Rev*. B 47, 11230 (1993).
28. C. J. Howard, "The approximation of asymmetric neutron powder diffraction peaks by sums of Gaussians," *J. Appl. Crystallogr*. 15, 15615 (1982).
29. W. Pitschke, H. Hermann, and N. Mattern, "The influence of surface roughness on diffracted X-ray intensities in Bragg–Brentano geometry and its effect on the structure determination by means of Rietveld analysis," *Powder Diff.* **8**, 74 (1993).
30. K. R. Rao, H. Ehrenberg, G. Markandeyulu, U. Varadaraju, M. Venkatesan, K. Suresh, V. Murthy, P. Schmidt and H. Fuess, "On the Structural and Magnetic Properties of $R_2Fe_{17-x}(A,T)_x$ (R = Rare Earth; A = Al, Si, Ga; T = Transition Metal) Compounds," *physica status solidi (a),* vol. **189**, no. 2, p. 373–388, February 2002.
31. H. Yan-ming, Y. Qi-wei, Z. Pan-lin, S. Xiang-dong, W. Fang-wei and S. Bao-gen, "Magnetic properties of $Dy_2Fe_{17-x}Cr_x$ and $Er_2Fe_{17-x}Cr_x$ (x = 0-3) compounds," *Acta Phys. Sin.* , vol. 6, no. 6, 1997.
32. S. Chikazumi, C.D. Graham, "Physics of Ferromagnetism", Second Ed. Oxford *University Press*, New York, **94**, 2009.
33. G. J. Long, S. R. Mishra, O. A. Pringle, W. B. Y. Z. Hu, F. Grandjean, D. P. Middleton and K. H. J. Buschow, *J. Magn. Magn. Mater.*, vol. **176**, 1997.
34. Y. Zhang, J. I. Budnick, W. A. Hines, B. G. Shen and Z. Cheng, "Effect of Ga substitution on the Sm sublattice anisotropy in $Sm_2Fe_{17-x}Ga_x$ ($0<x<8$)," *J. of App. Phys.*, vol. **85**, no. 8, pp. 4663-4665, 1999.
35. K. R. Rao, H. Ehrenberg, G. Markandeyulu, U. Varadaraju, M. Venkatesan, K. Suresh, V. Murthy, P. Schmidt and H. Fuess, "On the Structural and Magnetic Properties of $R_2Fe_{17-x}(A,T)_x$ (R = Rare Earth; A = Al, Si, Ga; T = Transition Metal) Compounds," *physica status solidi (a),* vol. **189**, no. 2, p. 373–388, February 2002.
36. J. J. Bara, A. T. Pedziwiatr and W. Zarek, "Investigations of crystal and magnetic properties of Dy-Fe intermetallic compounds," *J. Magn. Magn. Mater.*, vol. **27**, no. 2, p. 168–174, May 1982
37. M. Valeanu, N. Plugaru, and E. Burzo, "Effect of nitrogenation on the magnetic properties of $Y_2Fe_{17-x}M_x$ compounds, with M = Al, Ga or Si," *Solid State Commun.* **89**, 519 (1994).
38. L. Neél, "Propriétés magnétiques de l'état métallique et énergie d'interaction entre atoms magnétiques," *Ann. Phys. (Paris),* **5**, 232 (1936).
39. Z. W. Li and A. H. Morrish "Negative exchange interactions and Curie temperatures for Sm_2Fe_{17} and $Sm_2Fe_{17}N_y$," *Phys. Rev. B* **55**, 3670 (1997).
40. F. Grandjean, O. Isnard, and G. J. Long, "Magnetic and Mossbauer spectral evidence for the suppression of the magnetic spin reorientation in Tm_2Fe_{17} by deuterium", *Phys. Rev. B* **65**, 064429 (2002).
41. G. J. Long, O. Isnard, and F. Grandjean, "A Mossbauer spectral study of the magnetic properties of Ho_2Fe_{17} and $Ho_2Fe_{17}D_{3.8}$" *J. Appl. Phys.* **91**, 1423 (2002).